International Information and Engineering Technology Association
Advancing the World of Information and Engineering

Revue des Composites et des Matériaux Avancés-Journal of Composite and Advanced Materials
Vol. 31, No. 6, December, 2021, pp. 335-340
Journal homepage: http://iieta.org/journals/rcma

Lattice Parameters, Electronic, and Magnetic Properties of Cubic Perovskite Oxides $ARuO_3$ (A=Sr, Rb): A First-Principles Study

Ahmed Memdouh Younsi[1,2*], Lakhdar Gacem[2], Mohamed Toufik Soltani[1]

[1] University of Biskra, Laboratory of Physics of Photonics and Multifunctional Nanomaterials, BP 145, RP, Biskra 07000, Algeria

[2] Materials Science and Informatics Laboratory, University of Ziane Achour Djelfa, PostOffice Box 3117, Djelfa 17000, Algeria

Corresponding Author Email: ahmed.younsi@univ-biskra.dz

https://doi.org/10.18280/rcma.310604

Received: 5 November 2021
Accepted: 20 December 2021

Keywords:
ab initio calculations, density-functional theory, cubic perovskites, ferromagnetic ground state, $RbRuO_3$

ABSTRACT

Trioxides of rubidium, strontium, and ruthenium belong to the family of alkali and alkaline earth ruthenates. $SrRuO_3$ crystallizes in various symmetry classes—orthorhombic, tetragonal, or cubic—whereas $RbRuO_3$ is perovskite (cubic) structured and crystallizes only in the cubic space group $Pm\bar{3}m$(No. 221). In this study, we investigated the structural stability as well as the electronic and magnetic properties of two cubic perovskites $SrRuO_3$ and $RbRuO_3$. We established the corresponding lattice parameters, magnetic moments, density of states (DOS), and band structures using *ab-initio* density-functional theory (DFT). Both compounds exhibited a metallic ferromagnetic ground state with lattice parameter values between 3.83 and 3.96 Å; $RbRuO_3$ had magnetic moments between 0.29 and 0.34 μ_B whereas $SrRuO_3$ had magnetic moments between 1.33 and 1.66 μ_B. This study paves way for further $RbRuO_3$ research.

1. INTRODUCTION

Owing to their physical and chemical properties, alkali and alkaline earth ruthenates play an important role in magnetics. With regard to this family of compounds, researchers have previously studied the superconductivity of Sr_2RuO_4 [1], the ferromagnetic transition in Ca_2RuO_4 [2], and the anti-ferromagnetic behavior of Na_2RuO_4 [3]. These compounds form different crystalline lattices as influenced by varying external conditions such as temperature. The lattices may be orthorhombic (space groups Pnma, Imma, etc. tetragonal (space group I4/mcm), or cubic ($Pm\bar{3}m$ space group) [4, 5].

Cubic perovskites (ABO_3) have been studied extensively in the last two decades. For example, Xiao et al. [6] reported lattice parameters between 3.50 and 3.61 Å for $SrSiO_3$. Tariq et al. [7] theoretically computed lattice parameters between 3.80 and 3.85 Å for cubic perovskites of $SrAO_3$ (A = Cr, Fe, and Co).

$SrRuO_3$ has been observed to crystallize into a cubic perovskite structure at temperatures as high as 1273 K [4]. In their study on thin films, Choi et al. [5] demonstrated that a cubic perovskite structure ($Pm\bar{3}m$ space-symmetry group) can be obtained upon annealing $SrRuO_3$ at 950 K.

$SrRuO_3$ is a metallic oxide that exhibits both electronic and magnetic characteristics owing to the transition metal ruthenium [4, 8]. The theoretical study conducted by Granas et al. [9] investigated the magnetic and electronic properties of the orthorhombic and cubic structures of $SrRuO_3$.

Rubidium is an important alkali metal; located alongside strontium in period VI of the periodic table, rubidium has a large number of valence electrons and consequently has various electrical, electronic, and chemical applications [10].

In their pioneering work, Fischer et al. synthesized rubidium oxoruthenate (Rb_2RuO_4) from rubidium peroxide and ruthenium dioxide and also calculated its magnetic properties [11]. The trioxide of rubidium and ruthenium ($RbRuO_3$) decomposes to Rb_2RuO_4 and RuO_2, where RuO_2 crystallizes with tetragonal rutile structure ($P4_2/mmm$) [12], whereas Rb_2RuO_4 crystallizes with an orthorhombic structure (Pnma) [11]. These products, under certain physical–chemical circumstances such as thermal treatment, combine to produce the perovskite $RbRuO_3$ in $Pm\bar{3}m$ space-symmetry group [4, 13].

To the best of our knowledge, the cubic perovskite $RbRuO_3$ has yet to be synthesized in experiments or studied theoretically; so far, the material has only been simulated [13]. Pearson simulated it and determined its properties such as lattice parameters, elasticity, and band structure using VASP code and generalized gradient approximation (GGA). Accordingly, we investigated the similarities between $SrRuO_3$ and $RbRuO_3$; we compared their structural stability as well as electronic and magnetic properties. To this end, we employed several *ab-initio* methods from the density-functional theory (DFT) implemented in the CASTEP (Cambridge Serial Total Energy Package) code.

The rest of the paper is devoted to presenting some computational aspects and details of the proposed approach followed by a description of the simulation results and a discussion of key findings. Finally, we conclude by retracing the important findings of our work.

2. COMPUTATIONAL METHODOLOGY

We investigated the structural stability, electronic and magnetic properties of the $RbRuO_3$ and $SrRuO_3$ perovskites with space-group number 221 ($Pm\bar{3}m$). All calculations presented in this paper were performed using CASTEP [14]. CASTEP utilized DFT to compute the solution of the Schrödinger equation. The electron wave functions were developed on a plane-wave basis via periodic boundary conditions and Bloch's theorem.

Bloch's theorem [15] states can be written as Eq. (1).

$$\psi_{i,K}(r) = u_j(r)e^{iK.r} \tag{1}$$

$u_i(r)$ is a function that defines the periodicity of the potential. For example, $u_i(r+L)=u_i(r)$, where L is the length of the unit cell and K is a wavevector confined to the first Brillouin region. As $u_i(r)$ is a periodic function, we can express its Fourier expansion as Eq. (2).

$$u_j(r) = \sum_G C_j, Ge^{iG.r} \tag{2}$$

The reciprocal lattice vectors are defined by $G.R = 2\Pi m$, where m is an integer and R is a real-space lattice. C_i and G are plane-wave expansion coefficients. Therefore, the wave functions of the electron can be written as a linear set of plane waves.

$$\psi_{j,K}(r) = \sum_G C_{j,K+G}e^{i(K+G).r} \tag{3}$$

Brillouin zone integration and the Monkhorst–Pack scheme were adopted to determine the energy-band structure of the studied material using special k-points and the 6×6×6 grids of a 340-eV plane-wave cut-off. CASTEP used the Monkhorst–Pack scheme [16] to sample the Brillouin zone. After applying a series of convergence tests, we designated 340 eV as the energy cut-off. Further, we designated 10 k-points corresponding to the 6×6×6 Monkhorst–Pack meshes as a sampling of the first Brillouin zone. Self-consistent field algorithms were implemented in the CASTEP code to determine the electronic ground state of the systems studied. With the same code, the total energy of the systems was minimized via Vanderbilt ultrasoft pseudo-potentials [17, 18] and exchange-correlation functionals from GGA. The following exchange-correlation functionals were employed: Perdew–Burke–Erzerhof (PBE) [19], PBEsol (PBE for solids) [19, 20], Wu–Cohen functional (WC) [21], and Perdew–Wang (PW91) [22]. In addition, we employed local-spin-density approximation (LSDA) [23, 24], and LSDA with Hubbard correction (LSDA+U) [25, 26].

3. RESULTS AND DISCUSSION

3.1 Lattice parameters

Before calculating the electronic and magnetic properties, we adjusted the lattice parameters. The cube in Figure 1 illustrates the atomic positions in the primitive cell of the crystal lattice. Based on the Wyckoff positions for group $Pm\bar{3}m$, the ruthenium atom was placed at the center of the cube, Ru (0.5, 0.5, 0.5); atom A (A = Rb, Sr) was placed at each corner of the cube, 8A (0, 0, 0); and the oxygen atom was placed at the center of each face, $2O_1$(0, 0.5, 0.5), $2O_2$ (0.5, 0.5, 0), $2O_3$ (0.5, 0, 0.5) [27].

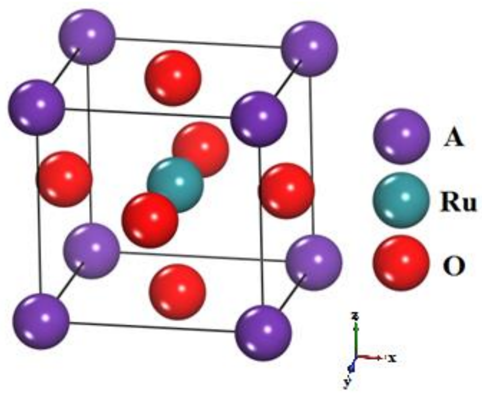

Figure 1. Crystal structure of primitive cell of ($ARuO_3$; A = Rb, Sr) in cubic system $Pm\bar{3}m$ (No. 221)

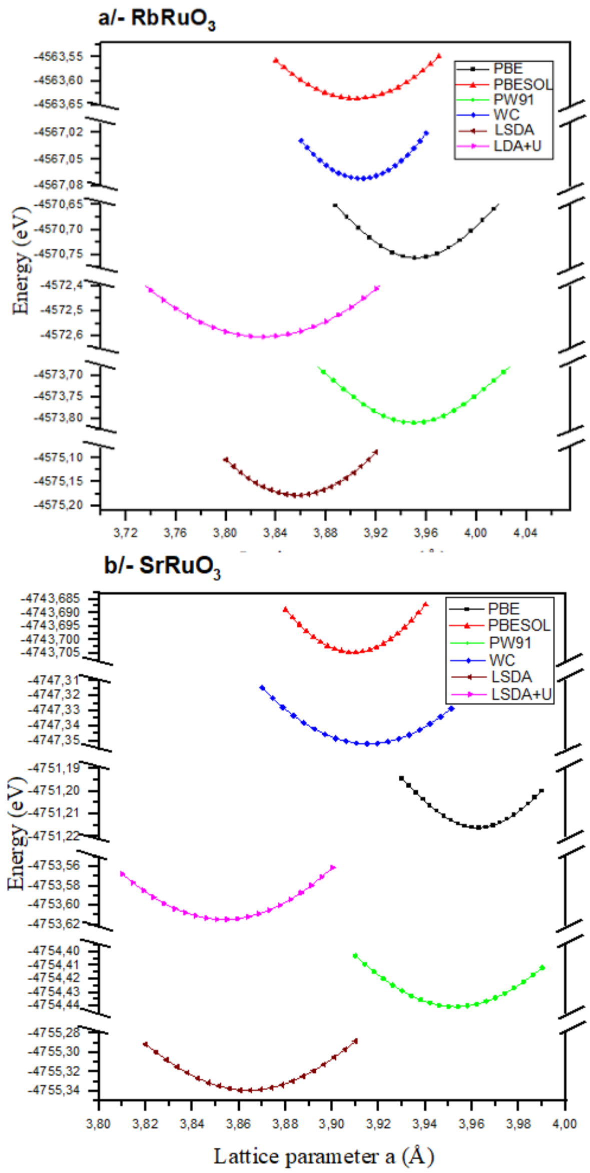

Figure 2. Structural parameter as a function of the energy of cubic perovskite; a) $RbRuO_3$ and b) $SrRuO_3$, using the Hubbard correction U = 1.0 eV

First, we used GGA and LSDA to optimize and calculate the equilibrium lattice constant (a_0) of the stable crystal structure of the primitive cell; for LSDA, we applied a high spin polarization on the ruthenium atom. As shown in Figures 2 a and b, the lattice parameters were traced as a function of energy, and through fitting, the curves were corrected according to the Birch–Murnaghan equation of state [28].

$$E(V)=E_0+\frac{9V_0B_0}{16}\left\{\left[\left(\frac{V_0}{V}\right)^{2/3}-1\right]B_0^{'}+\left[\left(\frac{V_0}{V}\right)^{2/3}-1\right]^2\left[6-4\left(\frac{V_0}{V}\right)^{2/3}\right]\right\} \qquad (4)$$

The equilibrium lattice parameter (a_0) was selected at ground state, *i.e.*, when the energy resulting from all interactions between electrons and ions in the studied systems was the lowest. Table 1 lists the results for the equilibrium lattice parameter and ground-state energy of the studied crystals according to the different functional calculation techniques. Furthermore, we observed that GGA is better than LSDA at estimating ionic bonding in molecular systems.

For $RbRuO_3$, we obtained lattice parameter values between 3.83 and 3.95 Å; these values were similar to those for $SrRuO_3$, which ranged between 3.85 and 3.96 Å. Notably, the $SrRuO_3$ values are consistent with the experimental results of Cuffini et al. [4] and theoretical findings of Abbes and Noura [27], as shown in Table 1. We also calculated the bulk moduli; we obtained values between 287 and 298 GPa for $RbRuO_3$, and between 278 and 291 GPa for $SrRuO_3$. Among the various computational methods, GGA–PBE yielded the most optimal results.

3.2 Electronic structure and magnetic properties

3.2.1 Density of states and magnetic moments

The transition metal ruthenium is responsible for the magnetic nature of $SrRuO_3$ and $RbRuO_3$. In this study, we applied ferromagnetic ordering, which is suitable for cubic ground states prior to ferromagnetic ordering; the structures with Pm$\bar{3}$m space-symmetry group. In this regard, we applied high spin-up and high spin-down polarization on the ruthenium atom. We then calculated the magnetic moments of the materials. The results are presented in Table 2.

For $SrRuO_3$, we obtained total magnetic moments between 1.33 and 1.66 μ_B; these results are in good agreement with those reported in other works [9, 29]. For $RbRuO_3$, the magnetic moments were lower, between 0.29 and 0.34 μ_B. As previously mentioned, there are no published articles reporting the laboratory synthesis or the theoretical examination of this compound. As such, we could not compare the corresponding results with known benchmarks. We noted that these two compounds had ferromagnetic ground-state energies shown in Tables 1 and 2 decreased after ferromagnetic ordering.

Figure 3 shows the total- and partial-density-of-states (TDOS and PDOS) curves of our materials. These results were obtained using the GGA–PBE functional with high spin-up and spin-down polarization.

We observed that the electron states were distributed on $2s^2$ and $2p^4$ orbital configurations for oxygen atoms; $4s^2$, $4p^6$, and $5s^1$ for rubidium atoms; $4s^2$, $4p^6$, and $5s^2$ for strontium atoms; and $4s^2$, $4p^6$, $4d^7$, and $5s^1$ for the ruthenium atoms. The Fermi level was fixed at 0 eV, where the overlap was clear at this level. We observed a metallic ground state for both compounds. For $RbRuO_3$, this metallic nature was attributed to the contribution of the electron states of the $5s^1$ orbital of Rb, the $2p^4$ orbital of O, and the $4d^7$ orbital of Ru. Conversely, for $SrRuO_3$, the electrons of the $5s^2$ orbital of Sr, the $2p^4$ orbital of O, and the $4d^7$ orbital of Ru contributed to the metallic behavior. A more detailed illustration of this metallic ground state presented in the band–structure curves.

Table 1. Equilibrium lattice parameter a_0 calculated via different methods in conjunction with GGA (without spin polarization) and LSDA (with Hubbard correction U = 1.0 eV)

Exchange–Correlation DFT functional E_{xc}	$RbRuO_3$ Ground-state energy (eV)	Lattice constant a_0 (Å)	Bulk modulus B_0(GPa)	$SrRuO_3$ Ground-state energy (eV)	Lattice constant a_0 (Å)	Bulk modulus B_0(GPa)
PBE	-4570.75	3.95	298.59	-4751.21	3.96	278.85
PBEsol	-4563.63	3.90	274.31	-4743.70	3.91	291.09
PW91	-4573.81	3.95	267.96	-4754.44	3.95	280.10
WC	-4567.07	3.91	286.65	-4747.35	3.91	290.08
LSDA	-4575.17	3.85	289.85	-4755.34	3.86	293.89
LSDA+U	-4572.60	3.83	287.46	-4753.61	3.85	291.74
Experimental					3.96 [4]	
Theoretical					3.87-3.97[27]	163-213 [27]

Table 2. Total magnetic moments M_{tot} calculated by different methods in conjunction with GGA (with high spin-up and spin-down polarization) and LSDA (with Hubbard correction U = 1.0 eV)

Exchange–Correlation DFT functional E_{xc}	$RbRuO_3$ Ground-state energy (eV)	$\lvert M_{tot}(\mu_B)\rvert$	$SrRuO_3$ Ground-state energy (eV)	$\lvert M_{tot}(\mu_B)\rvert$
PBE	-4570.76	0.340	-4751.36	1.665
PBEsol	-4563.65	0.318	-4743.82	1.423
PW91	-4573.82	0.335	-4754.58	1.595
WC	-4567.08	0.326	-4747.48	1.489
LSDA	-4575.17	0.267	-4755.34	1.332
LSDA+U	-4572.60	0.290	-4753.61	1.334
Experimental				1.190 [29]
Theoretical				1.320–1.800 [9]

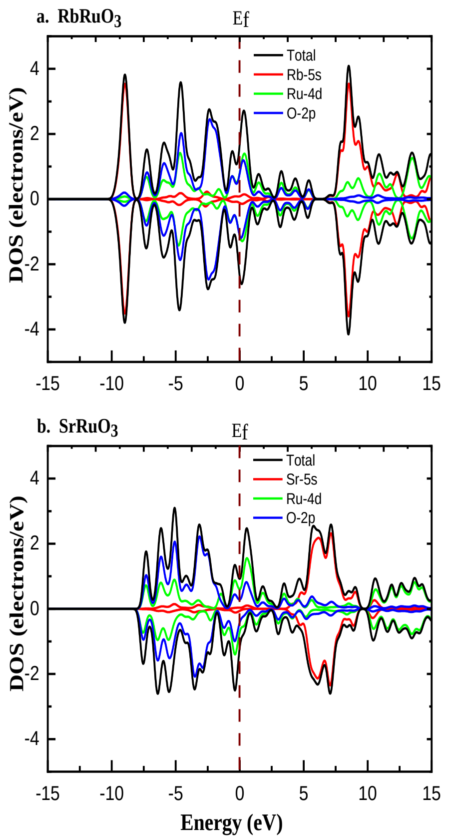

Figure 3. PDOS and TDOS using GGA–PBE functional with spin-up and spin-down polarization

3.2.2 Band structures

The outcome of the band–structure calculations is shown in Figures 4 and 5. For these computations, we used the GGA–PBE functional with and without spin polarization; the energy eigenvalues of the systems under consideration were traced using a function of reciprocal-space k-points. The Brillouin zones are defined at four zones in our calculation because the materials studied here crystallize in the cubic symmetry system. We observed overlapping of valence and conduction bands at Fermi level as well as at the end of the second and third Brillouin zones. This overlap is visible—with and without spin polarization—at the points between M and Γ (see Figures 4 and 5).

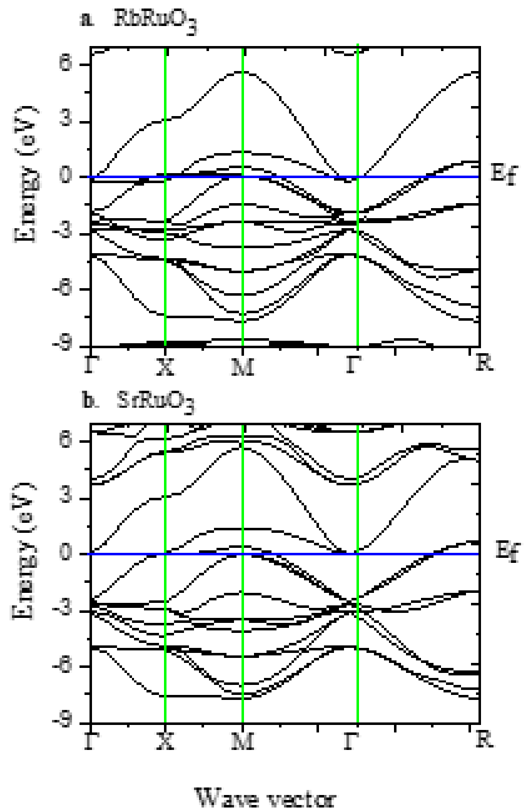

Figure 4. Band structure, using GGA–PBE functional without spin polarization

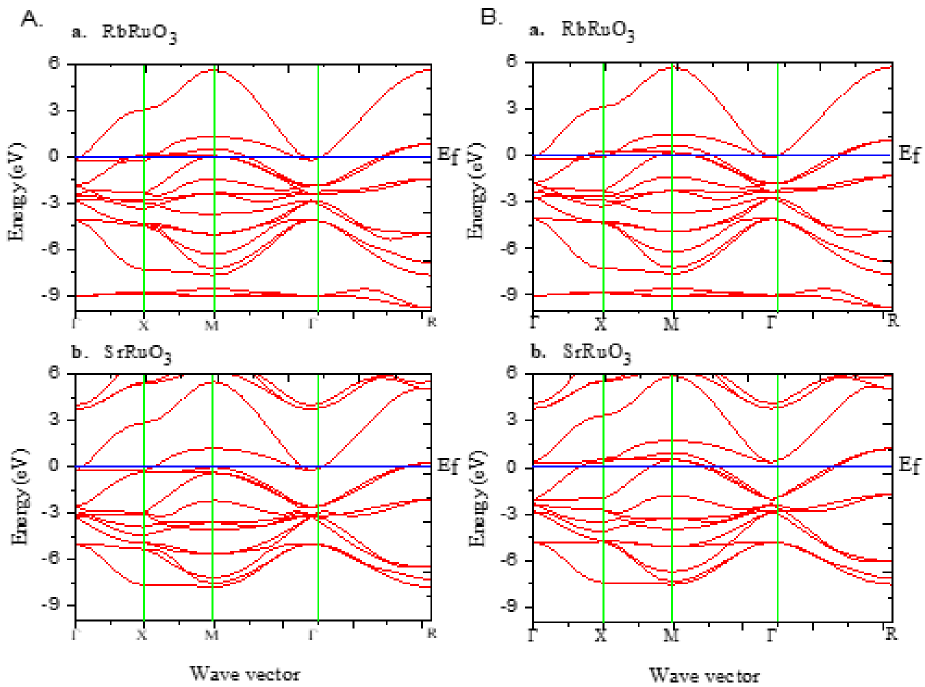

Figure 5. Band structure with A. spin-up polarization and B. spin-down polarization, using GGA–PBE functional

For $RbRuO_3$, the maximum energy values of the valence bands were found to be 0.556, 0.502, and 0.681 eV without spin polarization, with spin ascent, and with spin descent, respectively, whereas the corresponding minimum energy values of the conduction bands were -0.236, -0.254, and -0.148 eV.

Similarly, for $SrRuO_3$, the maximum energy values of the valence bands were 0.425, -0.007, and 0.963 eV, whereas the minimum energy values of the conduction bands were 0.008, -0.256, and 0.332 eV. These values indicate a larger overlap between the two bands. So, there are no band gaps. We conclude that all the specimens studied here are conductors.

4. CONCLUSION

We used *ab-initio* DFT calculations to determine the electronic and magnetic properties of two cubic perovskite oxide compounds, $RbRuO_3$ and $SrRuO_3$, belonging to a family of alkali and alkaline earth ruthenates. We observed that both compounds had similar lattice parameter values. Moreover, both were ferromagnetic conductors. However, they had different degrees of magnetization; compared to $SrRuO_3$, $RbRuO_3$ had lower magnetic moments. This theoretical study confirmed that both $RbRuO_3$ and $SrRuO_3$ can potentially be used in ferromagnetic conductivity-based technologies, for example, in metallic ultra-thin nanoribbons and magnetic thin-film domains. Furthermore, $RbRuO_3$ may be useful in applications requiring a small magnetic moment, such as layered hetero-structures with magnetic/nonmagnetic layers. Laminated heterogeneous structures are composed of multiple ferromagnetic and nonmagnetic layers. These composites have potential applications in spintronics, and several investigations—including interface magnetism, interlayer exchange coupling, and magnetization reversal from ferromagnetic to paramagnetic—have been conducted to this end. We believe our study will encourage experimental efforts to synthesize this compound.

ACKNOWLEDGMENT

The authors would like to thank the material science department team of the University of Biskra for funding this work.

REFERENCES

[1] Maeno, Y., Hashimoto, H., Yoshida, K., Nishizaki, S., Fujita, T., Bednorz, J.G., Lichtenberg, F. (1994). Superconductivity in a layered perovskite without copper. Nature, 372: 532-534. https://doi.org/10.1038/372532a0

[2] Nobukane, H., Yanagihara, K., Kunisada, Y., Ogasawara, Y., Isono, K., Nomura, K., Tanahashi, K., Nomura, T., Akiyama, T., Tanda, S. (2020). Co-appearance of superconductivity and ferromagnetism in a Ca_2RuO_4 nanofilm crystal. Sci. Rep., 10: 1-10. https://doi.org/10.1038/s41598-020-60313-x

[3] Mogare, K.M., Friese, K., Klein, W., Jansen, M. (2004). Syntheses and crystal structures of two sodium ruthenates: Na_2RuO_4 and Na_2RuO_3. Zeitschrift Fur Anorg. Und Allg. Chemie., 630(4): 547-552. https://doi.org/10.1002/zaac.200400012

[4] Cuffini, S.L., Guevara, J.A., Mascarenhas, Y.P. (1996). Structural analysis of polycrystalline $CaRuO_3$ and $SrRuO_3$ ceramics from room temperature up to 1273 K. Mater. Sci. Forum., 228-231: 789-794. https://doi.org/10.4028/www.scientific.net/MSF.228-231.789

[5] Choi, K.J., Baek, S.H., Jang, H.W., Belenky, L.J., Lyubchenko, M., Eom, C.B. (2010). Phase-transition temperatures of strained single-crystal $SrRuo_3$ thin films. Adv. Mater., 22(6): 759-762. https://doi.org/10.1002/adma.200902355

[6] Xiao, W.S., Tan, D.Y., Zhou, W., Liu, J., Xu, J. (2013). Cubic perovskite polymorph of strontium metasilicate at high pressures. Am. Mineral., 98: 2096-2104. https://doi.org/10.2138/am.2013.4470

[7] Tariq, S., Mubarak, A.A., Kanwal, B., Hamioud, F., Afzal, Q., Zahra, S. (2020). Enlightening the stable ferromagnetic phase of $SrAO_3$(A= Cr, Fe and Co) compounds using spin polarized quantum mechanical approach. Chinese J. Phys., 63: 84-91. https://doi.org/10.1016/j.cjph.2019.10.018

[8] Sahu, A.K., Dash, D.K., Mishra, K., Mishra, S.P., Yadav, R., Kashyap, P. (2018). Properties and applications of ruthenium. Noble Precious Met. - Prop. Nanoscale Eff. Appl., 17: 377-390. https://doi.org/10.5772/intechopen.76393

[9] Grånäs, O., Di Marco, I., Eriksson, O., Nordström, L., Etz, C. (2014). Electronic structure, cohesive properties, and magnetism of $SrRuO_3$. Phys. Rev. B - Condens. Matter Mater. Phys., 90(16): 1-11. https://doi.org/10.1103/PhysRevB.90.165130

[10] Butterman, B.W.C., Reese, R.G. (2003). Mineral Commodity Profiles – Rubidium. https://doi.org/10.3133/ofr0345

[11] Fischer, D., Hoppe, R., Mogare, K.M., Jansen, M. (2005). Syntheses, crystal structures and magnetic properties of Rb_2RuO_4 and K_2RuO_4. Zeitschrift Fur Naturforsch. - Sect. B J. Chem. Sci., 60: 1113-1117. https://doi.org/10.1515/znb-2005-1101

[12] Chen, R., Trieu, V., Schley, B., Natter, H., Kintrup, J., Bulan, A., Weber, R., Hempelmann, R. (2013). Anodic electrocatalytic coatings for electrolytic chlorine production: A review. Zeitschrift Fur Phys. Chemie., 227(5): 651-666. https://doi.org/10.1524/zpch.2013.0338

[13] Persson, K. Materials Data on $RbRuO_3$ (SG:221) by Materials project. DOE. Data. Explorer, OSTI, USA. https://doi.org/10.17188/1314744

[14] Segall, M.D., Lindan, P.J.D., Probert, M.J., Pickard, C.J., Hasnip, P.J., Clark, S.J., Payne, M.C. (2002). First-principles simulation: Ideas, illustrations and the CASTEP code. J. Phys. Condens. Matter., 14(11): 2717-2744. https://doi.org/10.1088/0953-8984/14/11/301

[15] Ashcroft, N.W., Mermin, N.D. (1976). Solid state: A new exposition. Science, 197(4305): 753. https://doi.org/10.1126/science.197.4305.753.a

[16] Pack, J.D., Monkhorst, H.J. (1977). “Special points for Brillouin-zone integrations” -a reply. Phys. Rev. B., 16(4): 1748-1749. https://doi.org/10.1103/PhysRevB.16.1748

[17] Vanderbilt, D. (1990). Soft self-consistent pseudopotentials in a generalized eigenvalue formalism. Phys. Rev. B., 41(11): 7892-7895. https://doi.org/10.1103/PhysRevB.41.7892

[18] Laasonen, K., Pasquarello, A., Car, R., Lee, C., Vanderbilt, D. (1993). Car-Parrinello molecular dynamics with Vanderbilt ultrasoft pseudopotentials. Phys. Rev. B., 47(16): 10142-10153. https://doi.org/10.1103/PhysRevB.47.10142
[19] Perdew, J.P., Burke, K., Ernzerhof, M. (1996). Generalized gradient approximation made simple. Phys. Rev. Lett., 77(18): 3865-3868. https://doi.org/10.1103/PhysRevLett.77.3865
[20] Perdew, J.P., Ruzsinszky, A., Csonka, G.I., Vydrov, O.A., Scuseria, G.E., Constantin, L.A., Zhou, X., Burke, K. (2008). Restoring the density-gradient expansion for exchange in solids and surfaces. Phys. Rev. Lett., 100(13): 1-4. https://doi.org/10.1103/PhysRevLett.100.136406
[21] Wu, Z.G., Cohen, R.E. (2006). More accurate generalized gradient approximation for solids. Phys. Rev. B - Condens. Matter Mater. Phys., 73(23): 2-7. https://doi.org/10.1103/PhysRevB.73.235116
[22] Perdew, J.P., Chevary, J.A., Vosko, S.H., Jackson, K.A., Pederson, M.R., Singh, D.J., Fiolhais, C. (1992). Atoms, molecules, solids, and surfaces: Applications of the generalized gradient approximation for exchange and correlation. Phys. Rev. B., 46(11): 6671-6687. https://doi.org/10.1103/PhysRevB.46.6671
[23] Ceperley, D.M., Alder, B.J. (1980). Ground state of the electron gas by a stochastic method. Phys. Rev. Lett., 45(7): 566-569. https://doi.org/10.1103/PhysRevLett.45.566
[24] Perdew, J.P., Zunger, A. (1981). Self-interaction correction to density-functional approximations for many-electron systems. Phys. Rev. B., 23(10): 5048-5079. https://doi.org/10.1103/PhysRevB.23.5048
[25] Anisimov, V.I., Zaanen, J., Andersen, O.K. (1991). Band theory and Mott insulators: Hubbard U instead of Stoner I. Phys. Rev. B., 44(3): 943-954. https://doi.org/10.1103/PhysRevB.44.943
[26] Shih, B.C., Yates, J.R. (2017). Gauge-including projector augmented-wave NMR chemical shift calculations with DFT+ U. Phys. Rev. B., 96(4): 1-10. https://doi.org/10.1103/PhysRevB.96.045142
[27] Abbes, L., Noura, H. (2015). Perovskite oxides MRuO3 (M = Sr, Ca and Ba): Structural distortion, electronic and magnetic properties with GGA and GGA-modified Becke-Johnson approaches. Results Phys., 5: 38-52. https://doi.org/10.1016/j.rinp.2014.10.004
[28] Birch, F. (1947). Finite elastic strain of cubic crystals. Phys. Rev., 71(11): 809-824. https://doi.org/10.1103/PhysRev.71.809
[29] Kanbayasi, A. (1976). Magnetic properties of $SrRuO_3$ single crystal. J. Phys. Soc. Japan., 41(6): 1876-1878. https://doi.org/10.1143/JPSJ.41.1876